CONFORMAL MAPPING OF NUCLEI IN 3D TOMOGRAPHIC CELL IMAGES TO ASSESS SHAPE HETEROGENEITY

Vivek Nandakumar[1,2], Xing An[3,4], Yalin Wang[3], Roger Johnson[2], Deirdre Meldrum[1,2]

[1]School of Electrical, Computer, and Energy Engineering, Arizona State University, Tempe, Arizona
[2]Center for Biosignatures Discovery Automation, Biodesign Institute, Tempe, Arizona
[3]School of Computing, Informatics, and Decision Systems Engineering, Arizona State University, Tempe, Arizona
[4]School of Information and Electronics, Beijing Institute of Technology, Beijing, China

ABSTRACT

Nuclear shape and its heterogeneity are diagnostically important criteria used by pathologists in cancer diagnosis. Pathology assessment is currently qualitative and is based on 2D brightfield microscopy images. We propose an imaging informatics framework to quantify nuclear pleomorphism by statistical characterization of 3D nuclear shape. We applied optical projection tomographic microscopy (OPTM) to image individual hematoxylin and eosin-stained cells with isotropic, sub-micron spatial resolution. We used adaptive thresholding schemes to segment cells and nuclei, and applied spherical conformal mapping methods on the 3D nuclear masks to compute 256 rotation invariant coefficients as shape descriptors for each nucleus. As a first application, we tested our methods on normal and cancerous epithelial cell lines derived from human esophagus and breast, analyzing 10 cell images per class. We applied ANOVA techniques to assess variations in nuclear shape within each cell type and among the four cell types. The automated segmentation was 96% accurate compared to manual tracing of the volumes of interest. Statistical analysis of shape coefficients revealed that cancer cell nuclei from both organs exhibited considerably larger variance in their coefficients relative to the corresponding normal cell nuclei. Our results demonstrate the promise of our methodology for the development of quantitative pathological assessments.

Index Terms— 3D cell imaging, computed tomography, shape analysis, conformal mapping, cancer, heterogeneity

1. INTRODUCTION

Nuclear structure and spatial genome organization are known to be altered in cancer [1, 2]. Nuclear pleomorphism is a characteristic trait exhibited by cancer cells and is a diagnostic parameter used by pathologists to assess malignancy. Conventional cancer diagnosis by pathologists involves visual assessment of nuclear structure and tissue architecture by 2D brightfield microscopy imaging of tissue sections stained with the absorption dyes hematoxylin and eosin. Pathologists qualitatively grade parameters such as nuclear shape, chromatin packing, number of mitoses, and cellular arrangement in the tissue. However, the efficacy and interoperator consistency of these morphological assessments is limited by their qualitative nature and the use of 2D microscopy to characterize 3D entities such as cells and tissue sections. Factors such as choice of focal plane, sample orientation and overlapping cells can obfuscate cellular detail and bias the diagnoses derived from 2D micrographs. Three-dimensional microscopy modalities, including confocal microscopy, that generate volumetric images by serially stacking 2D slices provide more information content than 2D widefield imaging, but are limited by the inherent anisotropy in spatial resolution between the lateral and the axial directions and have not penetrated clinical pathology practice patterns. Although extensive research has been undertaken in the field of computerized nuclear morphometry, few methods are available to quantitatively characterize nuclear shape variations. Nuclear roundness [3] or compactness [4] are the metrics most commonly applied to nuclear shape aberrations, but they are unitary values that only suggest global trends and cannot capture topological variations.

To overcome these limitations to precise and repeatable cell shape characterization, we developed a conjunctive framework utilizing optical projection tomographic cell imaging [5] followed by conformal mapping methods [6] to quantify nuclear shape. OPTM enables 3D imaging of individual cells with an isotropic spatial resolution of 350 nm. Spherical conformal parameterization provides a rotation invariant statistical representation of surfaces and thus allows unbiased comparative studies of arbitrary surfaces. The efficacies of cell computed tomography [7] and conformal mapping methods [6, 8, 9] have been been demonstrated separately in other studies. Here, we present the utility of a unified approach to assess nuclear pleomorphism. We algorithmically segmented the cell nuclei from OPTM images and applied spherical conformal parameterization to statistically characterize their 3D shape.

We computed 256 rotation invariant coefficients for every cell nucleus. We used our methods to assess the nuclear shape of normal and cancer cells in cell line models of the human esophagus and breast.

The remainder of this paper is organized as follows: In section 2, we describe our methods for image acquisition, 3D image processing, and spherical conformal mapping. We present our results in section 3 and offer conclusions and suggestions for future work in section 4.

2. METHODS

2.1. Cell imaging by OPTM

To prepare adherent epithelial cells (see section 3.1 for cell types) for tomographic imaging, we trypsinized cultured cells, resuspended them in appropriate media, immediately fixed the suspended cells with CytoLyt (Cytyc, Marlborough, MA), smeared them onto clean glass slides (VWR, West Chester, PA) coated with 0.01% Poly-L-Lysine (PLL; Sigma-Aldrich, St.Louis, MO) and stained them with 6.25% w/w hematoxylin and 1% w/w eosin dyes. We embedded the cells in an optical gel (Nye, Fairhaven, MA) and imaged them individually by OPTM using the Cell-CT instrument (VisionGate, Phoenix, AZ) to obtain 3D cell images with isotropic spatial resolution. The image acquisition procedure is detailed in [10]. Briefly, each volumetric cell image was generated by parallel filtered backprojection image reconstruction of 500 equi-angular optical absorption projections of the stained cell acquired over a 360-degree rotation. The 147-nm voxel matrix dimensions of a cell image were dependent on the cell size.

2.2. Segmentation

Image segmentation is a subject of extensive research, with many techniques available for 2D and 3D images. Our goal for the segmentation was to generate accurate binary nuclear masks for shape analysis. The contrast imparted to cell structures by the stains (hematoxylin for the nucleus and eosin for the cytoplasm) produced 3D images with high signal-to-noise ratio. Thus, optical density histogram-based segmentation methods sufficed to obtain accurate volumes of interest (VOIs). However, since every cell has a unique staining pattern, we used adaptive thresholding techniques to automatically delineate the cell and nuclear boundaries. We applied a unimodal thresholding scheme [11] to compute the cell boundary and 3-level Otsu thresholding [12] to compute the nuclear boundary. We computed the 3-level Otsu threshold on the segmented cell volume and chose the highest threshold intensity to delineate the nucleus. Finally, we applied a connected component labeling algorithm with 26-neighbor connectivity constraint to generate the 3D masks for our VOIs. Nuclear volumes ranged from 300, 000 to 500, 000 voxels depending on cell type. To validate the algorithmically computed cell and nuclear masks, we manually traced the cell and nuclear boundaries using Volview software (Kitware, Clifton Park, NY).

2.3. 3D nuclear shape characterization

We applied conformal geometry and spherical harmonics (SPH) analysis on the nuclear masks to statistically characterize nuclear shape. Conformal mapping is one-to-one, onto, and angle-preserving. Therefore, this method is appropriate for shape analysis on arbitrary surfaces. As detailed in [13], our shape characterization procedure is composed of three steps: (1) spherical conformal parameterization as detailed in [6], (2) computation of SPH coefficients with the help of a spherical fast Fourier transformation (FFT), and (3) computation of shape invariants from SPH coefficients.

We modeled the nuclear surface as a genus zero surface since harmonic maps are equivalent to conformal maps for closed genus zero surfaces. With a variational framework, we minimized the harmonic energy by solving the partial differential equation $\Delta_s = 0$, where S represents the spherical domain. We took a Gauss map as the initial map then used a steepest descent method to minimize the harmonic energy. At each step, we took the absolute derivative directions to constrain each surface point moving along the sphere's tangent directions [6]. In contrast to other methods, our method directly operates on spherical surface and thus the results are numerically more accurate.
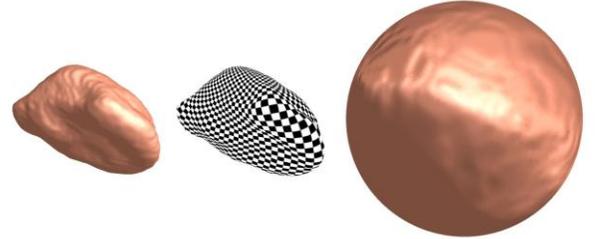

Fig.1. Spherical conformal parameterization for a nuclear surface. The nuclear surface (left) is conformally mapped to a sphere (right). Conformality is illustrated by texture mapping a checkerboard pattern from a sphere to the nuclear surface. The angle preserving property of conformal mapping maintains right angles on the checkerboard.

Figure 1 illustrates spherical conformality for a cell nucleus. The shading effects roughly illustrate the conformal mapping from the original surface to the sphere.

To compare nuclear shapes, we applied spherical harmonic analysis to generate a shape invariant representation of cell nuclei. This technique maps the nuclear surface topology onto a unit sphere using specialized spherical harmonic basis functions $f : S^2 \rightarrow C$ that take the form: $Y_l^m(\theta, \phi) = \sqrt{\dfrac{(2l+1)(l-m)!}{4(l+m)!}} P_l^m(\cos\theta)e^{im\phi}$

for degree m and order l, and $P_l^m(x)$ is the associated Legendre polynomial. A projection of a function $f \in L_2(S^2)$ onto this basis yields SPH coefficients $\hat{f}(l,m) = \langle f, Y_l^m \rangle_2$. Upon spherical conformal mapping, the original nuclear surface that is represented in Cartesian coordinates (x, y, and z) is now represented by a set of three functions $f_x, f_y, f_z : S^2 \to R$ defined on the sphere. To parameterize the nuclear surface, each of the three functions was represented by a set of SPH coefficients obtained by expanding a spherical FFT of the function. These SPH coefficients were used to compute the set of 256 shape invariants according to the formula:

$$s(l) = \sum_{i \in \{x,y,z\}} \sum_{|m| \le l} \| \hat{f}_i(l,m) \|^2 \quad l, l \in [1,256]$$

We used these 256 shape descriptors on used for our statistical shape analysis.

2.4. Statistical analysis

There are several ways to analyze the rotation invariant nuclear shape coefficients. As a first step toward understanding shape heterogeneity and its correlation with cell state (normal or cancerous), we performed two analyses. To assess intra-cell type shape heterogeneity, we computed the variance between shape coefficients among cells of the same type and determined the number of coefficients that had minimal variance ($<1\times10^{-11}$). To compare nuclear shapes between normal and cancerous cell types of each organ, we performed an ANOVA and tested for significance at $p<0.05$.

3. EXPERIMENTS AND RESULTS

3.1. OPTM reveals 3D nuclear shape heterogeneity

EPC2 (normal esophagus), Flo1 (invasive esophageal adenocarcinoma), HME1 (normal breast) and MDA-MB-231 (metastatic breast cancer) epithelial cells were cultured according to supplier protocols in T25 tissue culture flasks (BD Falcon, San Jose, CA). Cells were grown to ~80% confluence, then trypsinized and resuspended in 2 mL of medium. The cells were stained and imaged as described in section 2.1. Ten interphase cells of each cell type were analyzed.
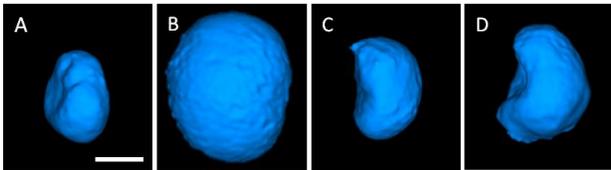

Fig. 2. Representative 3D pseudocolor renderings of nuclei imaged using optical projection tomography. (A), (B), (C), and (D) are nuclei of EPC2, Flo1, HME1, and MDA-MB-231 cells respectively. Differences in size and shape are apparent. Scalebar = 5 microns.

Representative volumetric cell images from the four cell types (see Fig. 2) illustrate typical variations in nuclear size and shape between the normal and cancer cells of both organs. Cancer cell nuclei were larger than their normal counterparts. Breast cell nuclei exhibited distinctly different shapes than the esophageal cell nuclei.
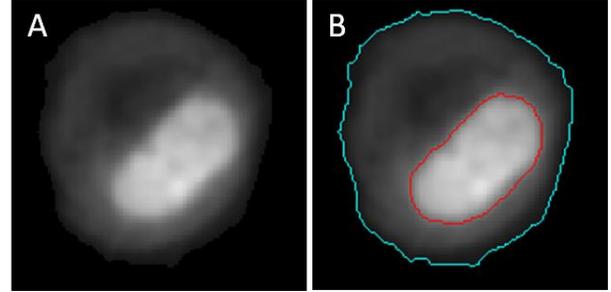
3.2. 3D segmentation

Fig. 3. 2D contour from 3D segmentation result (B) overlaid on a slice (A) of the 3D cell volume. Cell boundary is cyan and nuclear boundary is red.

Figure 3 shows a representative result of our segmentation techniques. We computed four metrics – DICE coefficient, Jaccard similarity index (JSI), Sensitivity (sens) and Specificity (spec) [14] to evaluate the efficacy of our segmentation methods. The results for the 40 cell images are summarized in Table I.

Table I: Evaluation of 3D segmentation methods

Cell type	VOI	Metrics (Average %)			
		DICE	JSI	sens	spec
EPC2	Cell	98.4	97	99.2	99.3
	Nucleus	96.6	93.6	96.7	99.8
Flo1	Cell	93.9	88.6	98.3	96.2
	Nucleus	90.9	83.9	85.4	99.9
HME1	Cell	98.7	97.5	99	99.5
	Nucleus	98	96.1	99.2	99.8
MDA-MB-231	Cell	97	94.7	99.7	98.1
	Nucleus	93.6	88.5	99.5	99.3

Table I indicates that our segmentation techniques performed reasonably well. Cancer cells (Flo1 and MB-231) were more challenging to segment accurately than their normal counterparts. This may be attributed to the underlying biology that results in less uniform staining of the cell membrane and nucleus in cancer cells.

3.3. 3D nuclear shape analysis by conformal mapping

Representative results of spherical conformal parameterization are shown in Fig. 4. The shape heterogeneity assessment enumerated in Table II indicates that in both esophagus and breast the normal cells exhibited considerably greater similarity in their nuclear shape than the cancer cells. Flo1 cell nuclei exhibited the largest shape heterogeneity. The ANOVA tests determined the means of 251 nuclear shape coefficients to be significantly different

between the EPC2 and Flo1 cell types and 77 coefficients to be significantly different between the HME1 and MDA-MB-231 cells. This suggests that nuclear shape alterations may be more pronounced in esophageal than in breast cancer.
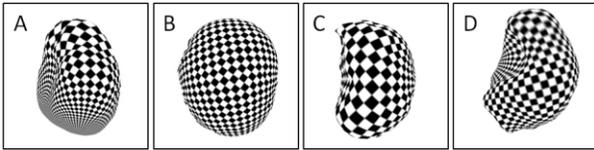

Fig. 4. Conformal parameterizations corresponding to nuclei in Fig. 2. The conformal map is visualized by texture mapping a checkerboard pattern onto the nuclear mask surface. The right angles show the angle preserving property of our mapping.

Table II: Shape heterogeneity analysis

Cell type	Proportion of similar shape coefficients(%)
EPC2	62.5
Flo1	31.6
HME1	60.9
MDA-MB-231	48.0

4. CONCLUSIONS AND FUTURE WORK

We presented imaging technology and informatics methods to quantitatively assess 3D nuclear shape, demonstrating their efficacy in quantifying nuclear shape heterogeneity within a cell type, and suggesting their promise for capturing pleomorphic variations between normal and cancer cells. Tomographic cell imagery with isotropic spatial resolution enabled accurate representation of 3D nuclear shape. The segmentation methods automatically and accurately defined nuclear VOIs within the cell images. Application of conformal geometry and spherical harmonics analysis methods to describe nuclear surface geometry by a series of spherical harmonic coefficients enabled representation and quantitative comparison of nuclear shapes by rotation invariant shape descriptors.

Results of this pilot study validate current knowledge concerning the considerable nuclear pleomorphism in cancer cells and the changes in nuclear morphology as cells transform from normal to malignant state. The extent of shape heterogeneity we found in normal cells (EPC2 and HME1) is noteworthy. This study highlights the promise of these quantitative methods for application to clinical pathology and cellular heterogeneity investigations. The proposed framework facilitates numerous extensions for analysis. Our short term future goal is to apply this framework on a larger image dataset to perform automated nuclear shape-based classification of cells.

5. ACKNOWLEDGMENTS

6. REFERENCES

[1] N. V. Marella, S. Bhattacharya, L. Mukherjee *et al.*, "Cell type specific chromosome territory organization in the interphase nucleus of normal and cancer cells," *Journal of cellular physiology,* vol. 221, no. 1, pp. 130-138, 2009.

[2] D. Zink, A. Fischer, and J. Nickerson, "Nuclear structure in cancer cells," *Nature Reviews Cancer,* vol. 4, pp. 677-687, 2004.

[3] R. W. Veltri, S. Isharwal, M. C. Miller *et al.*, "Nuclear roundness variance predicts prostate cancer progression, metastasis, and death: A prospective evaluation with up to 25 years of follow-up after radical prostatectomy," *The Prostate,* vol. 70, no. 12, pp. 1333-1339, 2010.

[4] A. Huisman, L. Ploeger, H. Dullens *et al.*, "Development of 3D chromatin texture analysis using confocal laser scanning microscopy," *Cellular Oncology,* vol. 27, no. 5/6, pp. 335, 2005.

[5] Q. Miao, J. R. Rahn, A. Tourovskaia *et al.*, "Dual-modal three-dimensional imaging of single cells with isometric high resolution using an optical projection tomography microscope," *Journal of biomedical optics,* vol. 14, pp. 064035, 2009.

[6] X. Gu, Y. Wang, T. F. Chan *et al.*, "Genus zero surface conformal mapping and its application to brain surface mapping," *Medical Imaging, IEEE Transactions on,* vol. 23, no. 8, pp. 949-958, 2004.

[7] M. Meyer, M. Fauver, J. Rahn *et al.*, "Automated cell analysis in 2D and 3D: A comparative study," *Pattern Recognition,* vol. 42, no. 1, pp. 141-146, 2009.

[8] Y. Wang, L. M. Lui, X. Gu *et al.*, "Brain surface conformal parameterization using Riemann surface structure," *Medical Imaging, IEEE Transactions on,* vol. 26, no. 6, pp. 853-865, 2007.

[9] Y. Wang, J. Zhang, B. Gutman *et al.*, "Multivariate tensor-based morphometry on surfaces: Application to mapping ventricular abnormalities in HIV/AIDS," *Neuroimage,* vol. 49, no. 3, pp. 2141-2157, 2010.

[10] V. Nandakumar, L. Kelbauskas, K. F. Hernandez *et al.*, "Isotropic 3D nuclear morphometry of normal, fibrocystic and malignant breast epithelial cells reveals new structural alterations," *PloS ONE,* vol. 7, no. 1, pp. e29230, 2012.

[11] P. Rosin, "Unimodal thresholding," *Pattern Recognition,* vol. 34, no. 11, pp. 2083-2096, 2001.

[12] P. S. Liao, T. S. Chen, and P. C. Chung, "A fast algorithm for multilevel thresholding," *Journal of information science and engineering,* vol. 17, no. 5, pp. 713-728, 2001.

[13] B. Gutman, Y. Wang, J. Morra *et al.*, "Disease classification with hippocampal shape invariants," *Hippocampus,* vol. 19, no. 6, pp. 572-578, 2009.

[14] D. W. Shattuck, G. Prasad, M. Mirza *et al.*, "Online resource for validation of brain segmentation methods," *Neuroimage,* vol. 45, no. 2, pp. 431-439, 2009.